Journal of Power Sources 264 (2014) 22–29

Contents lists available at ScienceDirect

Journal of Power Sources

journal homepage: www.elsevier.com/locate/jpowsour

Cycling of soluble lead flow cells comprising a honeycomb-shaped positive electrode

A. Oury [a], A. Kirchev [a], Y. Bultel [b,*]

[a] Laboratoire de Stockage de l'Electricité, Institut National de l'Energie Solaire, Commissariat à l'Energie Atomique et Energies Alternatives (CEA-Liten), 50, avenue du Lac Léman - LYNX 3, BP332, 73377 Le Bourget du Lac, France
[b] Laboratoire d'Electrochimie et de Physico-chimie des Matériaux et des Interfaces (LEPMI) UMR 5291 CNRS/Grenoble – INP/UJF/UdS, 1130, rue de la piscine, BP 75, 38402 Saint Martin d'Hères, France

HIGHLIGHTS

- Soluble lead/acid flow cells with honeycomb-shaped positive electrode are cycled.
- A carbon/carbon composite substrate for the honeycomb leads to a poor cyclability.
- A graphite substrate for the honeycomb enhances the cell performance.
- Fluoride ions used as an additive in the electrolyte improve the adhesion of PbO_2.

ARTICLE INFO

Article history:
Received 22 December 2013
Received in revised form
2 April 2014
Accepted 11 April 2014
Available online 24 April 2014

Keywords:
Redox flow batteries
Soluble lead-acid flow battery
Honeycomb-shaped positive electrode
Cycling

ABSTRACT

In this study, soluble lead/methanesulfonic acid flow cells comprising a 3-D honeycomb-shaped positive electrode sandwiched between two planar negative electrodes are tested under galvanostatic cycling. Two types of materials are used for the honeycomb: homemade vitreous carbon/carbon composite and graphite. The cells comprising the C/C composite substrate shows a poor cyclability with coulombic and energy efficiencies below 80% and 50%, respectively, as well as a very limited lifetime. After a few tens of cycles, the cells cannot be discharged any longer due to the emergence of overvoltages associated with the passivation of the positive electrode in the discharged states. Using the graphite-based electrode, the cyclability is considerably improved: efficiencies of 95% in charge and 75% in energy are obtained, a hundred of cycles can be achieved and no passivation is observed. The cycle life of the cell is, however, limited by lead dendrite-like formation at the negative plates. Finally, this study shows that the incorporation of fluoride ions into the electrolyte improves greatly the adhesion of PbO_2 on the positive electrode surface upon cycling.

© 2014 Elsevier B.V. All rights reserved.

1. Introduction

Redox flow batteries (RFBs) are considered as a promising solution for the grid-connected storage of electricity, especially within smart-grids that involve intermittent renewable energy sources. The main advantages associated with the RFBs compared to the other electrochemical storage systems are, on one hand, the independence of the power and the energy that can be provided, which makes these systems very flexible and, on the other hand, the potentially low cost of each energy unit, especially for high-capacity systems.

Most of the RFB systems developed up to now (all-vanadium, iron–chromium, bromine–polysulphide, etc.) involve the use of an ionic exchange membrane for separating the active species of the positive and negative electrolytes. The membrane remains one of the most expensive part of these RFB systems [1], due to the numerous requirements to which it is subjected (selectivity, conductivity, chemical stability, etc.). Hence, a few technologies have been developed that do not require any separator. These are generally redox flow batteries involving the deposition of solid phase at both electrodes during charge. Among them, the soluble lead flow battery (SLFB) was proposed a few years ago by Pletcher et al. [2–11]. In this membrane-free system, lead(II) ions are highly soluble in MSA (methanesulfonic acid, (CH_3SO_3H)) and are deposited as solid Pb at the negative electrode and as PbO_2 at the positive electrode during the charge according to the following reaction:

* Corresponding author. Tel.: +33 (0)476826580.
E-mail address: Yann.Bultel@lepmi.grenoble-inp.fr (Y. Bultel).

http://dx.doi.org/10.1016/j.jpowsour.2014.04.058
0378-7753/© 2014 Elsevier B.V. All rights reserved.

$$2Pb^{2+}_{(aq)} + 2H_2O \underset{\text{discharge}}{\overset{\text{charge}}{\rightleftharpoons}} PbO_{2(s)} + Pb_{(s)} + 4H^+ \quad (1)$$

Some SLFB mono-cells comprising two planar facing electrodes with the electrolyte flowing in-between were designed and cycled [3,4,9]. The overall performances and the lifetime of the cells were found to be strongly limited by the electrochemistry of the PbO_2/Pb^{2+} couple. Due to its sluggish kinetics, the energy efficiency is limited to approximately 65%. Besides, the incomplete dissolution of PbO_2 leads to a coulombic efficiency comprised between 80% and 90% and to a progressive build-up of both PbO_2 and Pb on the electrodes responsible for the decrease in the Pb^{2+} concentration together with an increase in the H^+ concentration in the electrolyte upon cycling. As a consequence of the impoverishment in Pb^{2+} ions, the lifetime of the 10 cm × 10 cm-flow cell was reported to be 40 and 20 cycles at a current density of 20 and 30 mA cm^{-2}, respectively, with a charging time of 1 h in 1.5 L of a 0.5 L Pb(II) + 0.5 L CH_3SO_3H electrolyte [9].

Other failure modes were identified, including the formation of lead dendrites at the negative electrode, the creep of lead dioxide onto non-conductive surface like the electrolyte inlets or the shedding of lead dioxide particles from the electrode that accumulate into slow convective zones [9,11]. All of these dysfunctions can short-circuit the cell.

Using graphite electrodes, Verde et al. [12] reported coulombic and energy efficiencies of 95% and 79%, respectively, with a lifetime of 2000 cycles. It appeared that the dissolution of PbO_2 could be improved by both a high stirring rate of the electrolyte and a charging potential that encourages the formation of nano-sized PbO_2 particles. However, the cell configuration (cylindrical vessel with magnetic stirring, 2.5 cm × 3.5 cm electrodes) and the cycling conditions (consumption of less than 5% of the lead(II) ions during charge) are far from a realistic industrial operation.

As reported in our previous study concerning the mechanisms of PbO_2 cycling in MSA, the incomplete dissolution of lead dioxide appears to be a result of the formation of resistive sub-oxides, mentioned as PbO_x [13], during the reduction of PbO_2. At high acid concentrations (>1 mol L^{-1}), PbO_x may be formed within the bulk of the layer, owing to the diffusion of protons in the hydrated PbO_2 clusters, resulting in a passivation of the electrode, which cannot be further cycled. At moderate acidities (<1 mol L^{-1}), PbO_x is still formed but remains close to the surface of the layer. It was also suggested that the formation of PbO_x can be limited at low current density (2 mA cm^{-2}). On the basis of these observations, we proposed a novel three-dimensional geometry for the positive electrode, based on the honeycomb structure, which is likely to decrease the activation overvoltages together with reducing the formation of PbO_x [14]. A numerical model was implemented to predict the current distributions within the cell together with the voltage and the simulated data were in good accordance with the experiments. However, the dissolution of PbO_2 was found particularly limited in the experimental cells, suggesting the need for more investigations.

Therefore, the purpose of the present paper is to further analyse the behaviour of the honeycomb-based flow cell geometry under galvanostatic cycling conditions. Firstly, the cycling of vitreous carbon/carbon composite honeycomb cells is considered. Then, another kind of honeycomb electrode, made of graphite, is tested in the second part of the paper.

2. Experimental

The SLFB flow cell prototypes consist of a honeycomb-shaped positive electrode which is sandwiched between two planar negative electrodes as proposed in Ref. [14]. Two types of honeycomb substrates are used in this study: type (1) is a honeycomb structure made of a vitreous carbon composite material and type (2) is a "pseudo-honeycomb" structure made of graphite.

Electrodes of type (1) are obtained by the carbonisation, under inert atmosphere, of a carbon-based honeycomb block, following a similar protocol as described in Ref. [15]. The primary block, presented in Fig. 1, mainly consists of a honeycomb structure made of an *Aramid*® fibre paper impregnated with a phenol/formaldehyde resin, obtained from *Euro-Composite* under the catalogue reference *ECA-I 144*, with alveoli walls of ~100 μm in thickness. The honeycomb structure is embedded in a rigid frame (~2 mm thick) made of a phenolic resin-based mixture obtained by heating a mixture the *CELLOBOND*® *J2027L* phenolic resin (80 wt.%) from *Momentive Specialty Chemicals*, ethanol (12 wt.%), 60 μm-long milled carbon fibres (4 wt.%) from *Toho Tenax*, and the specific *CELLOBOND*® *Phencat 382* catalyst (4 wt.%) at a temperature of 60 °C during 24 h. The block is cut into slices that will constitute, after carbonisation, the conductive substrate of the positive electrode. The carbonisation is carried out in an oven with the following heating protocol: (1) a first temperature ramp is applied from 20 °C to 200 °C at 0.2 °C min^{-1} under air atmosphere for drying the sample, followed by (2) a second ramp from 200 °C to 1000 °C at 1.2 °C min^{-1} and under nitrogen atmosphere for carbonizing the structure. The oven is then switched off, the temperature decreases slightly and the sample is removed when it has reached the room temperature. The resulting material is a vitreous carbon/carbon composite with an electronic conductivity of ~7000 S m^{-1}. The mean diameter D_c of the honeycomb alveoli is about 2.7 mm, the depth L_c of the alveoli varies between 0.9 and 1.8 cm and the walls separating each alveoli are ~100 μm thick (see Fig. 2a).

Electrodes of type (2), presented in Fig. 2b, are obtained by machining an array of circular apertures (4 mm in diameter) in a graphite plate (1.27 cm in thickness) provided by *Alfa Aesar*. Due to the brittleness of the graphite, a substantial distance was kept between each aperture in order not to damage the structure while drilling, which decreases substantially the surface area developed by the electrode compared to the ideal honeycomb structure.

The positive electrode is assembled with two planar copper plates (negative electrodes) using the same assembly as described in Ref. [14]. A 6.5 cm × 4.5 cm-section of the positive electrode is exposed to the electrolyte using a PVC frame to mask the edges. In the case of the electrode of type (1), the ratio R_A between the active area of the positive electrode and that of the two planar negative plates is given by Ref. [14]:

$$R_A = \frac{2L_c}{D_c} \quad (2)$$

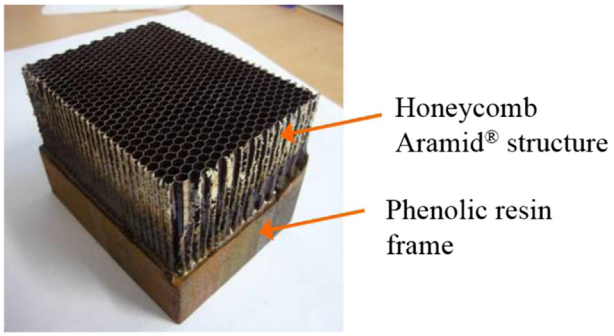

Fig. 1. Honeycomb-shaped block *ECA-I 144* from *Euro-Composites*, made up of an *Aramid*® matrix impregnated with a phenol/formaldehyde resin, embedded in the phenolic resin-based frame.

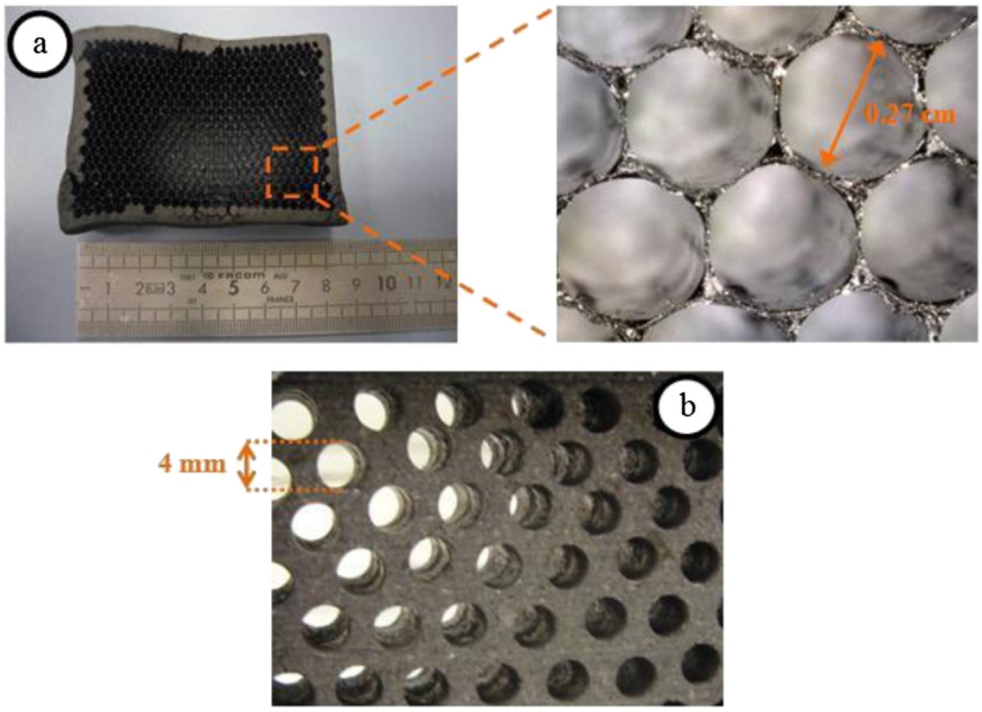

Fig. 2. (a) Vitreous carbon/carbon composite electrode of type (1) obtained by the carbonisation of the *Aramid*®/resin structure under nitrogen atmosphere. (b) Pseudo-honeycomb electrode of type (2) designed by drilling an array of circular apertures in a 1.27 cm-thick graphite plate.

The electrolyte flow is provided by a *KNF Lab Liquidport* diaphragm pump with the flow rate set at ~300 mL min^{-1}. Fig. 3 shows the experimental cell connected to the pump and the electrolyte reservoir. The galvanostatic cycles are prescribed with a *Biologic VSP-300* monitored by the *EC-Lab* software. An open circuit period of 30 min is applied after each charge and discharge.

The electrolytes are made from lead oxide powder (PbO 99%, *Sigma–Aldrich*) dissolved in a methanesulfonic acid solution (from MSA 70%, *Alfa-Aesar*). Hexadecyltrimethylammonium *p*-toluene sulfonate (HDTMA: $C_{16}H_{33}(CH_3)_3N{\cdot}C_7H_6SO_3H$) (5 mM) obtained from *Sigma Aldrich* is added to all of the electrolyte solutions, as an additive surfactant for lead deposition at the negative electrodes [6]. Sodium fluoride (NaF) (60 mM) was also added to the solutions to enhance the PbO_2 adhesion to the positive electrode during cycling [15]. Unless otherwise stated, the electrolyte composition is 1 M $Pb(CH_3SO_3)_2$ + 0.25 M CH_3SO_3H + 5 mM HDTMA + 60 mM NaF in the uncharged state.

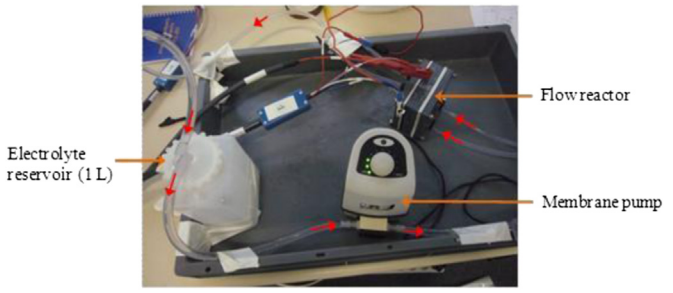

Fig. 3. Experimental cell connected to the membrane pump and the electrolyte reservoir. The red arrows represent the electrolyte flow. (For interpretation of the references to colour in this figure legend, the reader is referred to the web version of this article.)

3. Results and discussion

3.1. Cells with the C/C composite honeycomb-shaped positive electrode

3.1.1. Cycling with a high amount of deposits

A first cycling experiment was performed with a cell comprising a positive electrode of type (1). The depth of the honeycomb structure is 1.8 cm, giving to the positive electrode a geometric surface area which is 13-fold higher than that of the total negative plates area ($R_A = 13$). The current applied to the cell is 1.7 A, which corresponds to an average current density of 30 mA cm^{-2} at the negative plates and ~2.3 mA cm^{-2} at the positive electrode. The charging periods last 3 h and the discharges are prescribed until the cell voltage drops below 0.5 V. The electrolyte volume of 1 L gives a consumption of ~20% of the active soluble lead(II) species at each charge.

Fig. 4 shows the voltage response of the cell for the first 9 cycles. As it can be observed, the voltage transient displays a profile that is classically reported for SLFB cells. The first charge occurs at relatively constant voltage (~2.1 V) and the subsequent charges decompose into a first period associated with a low voltage and a second period where the voltage increases significantly until it reaches a plateau close to 2.1 V. This phenomenon was interpreted in a previous study by changes in the morphology of the deposited PbO_2-layer, which make both the local current density and the positive electrode polarization to vary [16]. Substantial voltage spikes are also observed as soon as the 5th charge, which can be associated with short-circuits between the electrodes arising by contacts between the deposits. After the 13th cycle, the cell was disassembled to observe the electrode surface, as presented in Fig. 5. A great amount of accumulated material can be seen on both electrodes. The lead deposit consists of thick aggregates stretching all over the copper surface regarding the honeycomb. A great amount of brown PbO_2 can be observed into the honeycomb alveoli, some of them being almost entirely obstructed.

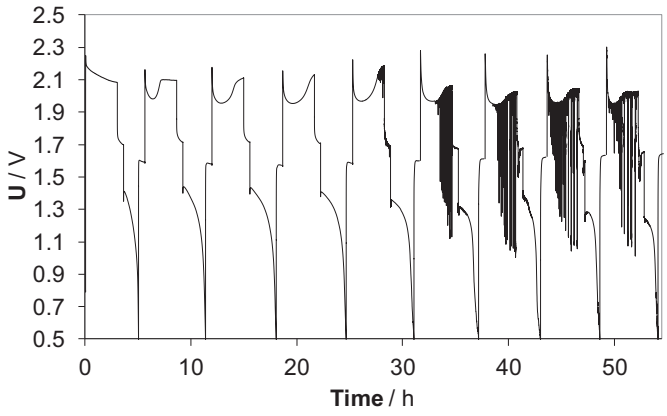

Fig. 4. Voltage response of the cell comprising a positive electrode of type (1) (1.8 cm thick) cycled at 1.7 A (30 mA cm^{-2} at the negative plates). Charges of 3 h with 1 L of electrolyte comprising 1 M $Pb(CH_3SO_3)_2$ + 0.25 M CH_3SO_3H + 5 mM HDTMA + 60 mM NaF in the uncharged state.

This phenomenon is clearly a result of the incomplete dissolution of lead dioxide as noticed in a previous study [14]. The average charge efficiency is 70% for the first 5 cycles and becomes even worth afterwards. This means that at least 30% of the deposited materials remain on the electrode surface at each cycle, leading to a great amount of accumulated materials as observed in Fig. 5.

3.1.2. Cycling with a low amount of deposits

In order to minimise the build-up of deposits upon cycling, the applied current and the charging time was decreased to 0.6 A and 2 h, respectively. The electrolyte volume was set at 0.5 L, which implies a consumption of ~10% of lead(II) during charge. The C/C composite positive electrode was 0.9 cm in depth, corresponding to an area ratio R_A of ~7. The voltage response of the 30 cycles that could be applied to the cell is given in Fig. 6, with focuses on cycles 1–6 and 18–23. It can be noticed a significant evolution of the voltage upon cycling. For the first six cycles (Fig. 6b), the average voltage values are 1.88 V and 1.33 V for charge and discharge, respectively. Surprisingly, during cycles 18–23 (Fig. 6c), the voltage has increased to 1.98 V in charge and decreased to 0.91 V in discharge, i.e. a significant additional overvoltage appears early in cycling. The discharges become even impossible after the 30th cycle.

Fig. 7 presents on one hand the evolution of the charge and the energy efficiencies of the cell (Fig. 7a.) and on the other hand the evolution of the internal resistance R_{int} (Fig. 7b.) throughout cycling. The charge efficiency is close to 80% at the early stage of cycling and decreases suddenly by the 20th cycle, due to the discharge failure. The energy efficiency, which is around 55% at the beginning of the experiment, decreases regularly from the 9th cycle to the end. This is due to the progressive appearance of the additional overvoltages.

The internal resistance measured after charge and that measured after discharge both drop gradually upon cycling. R_{int} decreases from 0.155 Ω, which is the value measured before the first charge, to 0.046 Ω after the 30th cycle. The evolution of R_{int} reflects the evolution of the electrolyte composition on account of the build-up of active species on the electrode surface. Before cycling, the electrolyte (1 M $Pb(CH_3SO_3)_2$ + 0.25 M CH_3SO_3H) has a conductivity of ~12 S m^{-1}. When the battery cycles, the composition evolves towards less Pb^{2+} and more H^+, which makes the electrolyte conductivity to rise significantly, mainly due to the release of protons [14]. The titration of the residual lead(II) in the electrolyte during the experiment gave a Pb^{2+} content of 0.6 M at mid-cycling and roughly 0 M at the end of cycling. At this time, the concentration in protons exceeds 2 M, giving a theoretical conductivity of more than 40 S m^{-1} [14]. This is in good accordance with the observed 70%-decrease in the internal resistance of the cell. Besides, the charge balance after cycling (~32,000C supplied to the cell in charge that are not discharged) is in good agreement with the observed complete depletion of lead(II) species in the electrolyte.

Electrochemical Impedance Spectroscopy (EIS) was also performed at open circuit after each OCV period following the charges and the discharges. Fig. 8 shows, as an example, the Nyquist diagrams recorded after the 10th charge and discharge. The spectrum obtained after charge basically consists in a first RC arc associated with a resistance of ~0.5 Ω (charge transfer process) followed by a low-frequency diffusion slope. The spectrum recorded after the discharge is completely different with the appearance of an incomplete but large RC semi-circle in the complex plane. The resistance associated is of the order of 3 Ω, i.e. 6 times higher than the charge transfer arc obtained after charge. It must be noted that all of the EIS spectra were found very similar for each cycle. Clearly, the cell seems to be in a passivated state after discharge and this must be related to the positive PbO_2-electrode. Indeed, the spectrum is very similarly to that observed after the dissolution of PbO_2 in highly acidic media [13]. Besides, a clear voltage peak is observed at the beginning of each charge, revealing the depassivation of the electrode as mentioned by Pavlov and Petkova [17] in the case of the classical Pb–H_2SO_4 battery. This peak was also observed at the beginning of the PbO_2 redeposition in our study of PbO_2 cycling in MSA medium (Fig. 3a of Ref. [13]). However, in the present case, the passivation cannot be strictly the result of the acidity since it occurs even during the early stage of cycling, i.e. when the protons concentration is still moderate in the electrolyte (<1 M).

3.1.3. Effects of fluoride ions

The previous experiments were all performed in the presence of 60 mM of NaF dissolved in the electrolyte since it has been shown

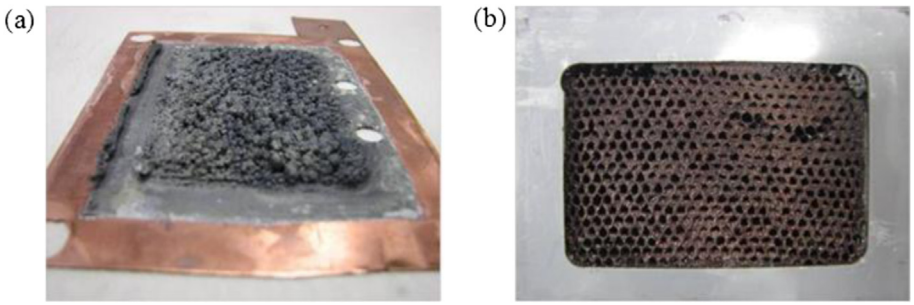

Fig. 5. Accumulation of (a) lead on the copper plate and (b) lead dioxide on the C/C honeycomb after the cycling presented in Fig. 4.

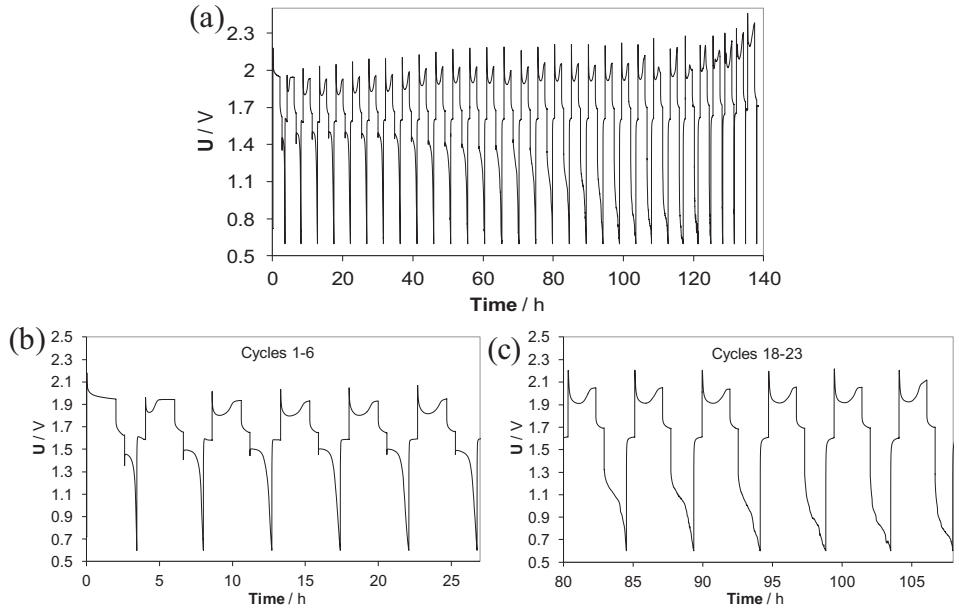

Fig. 6. Voltage response of the cell comprising a positive electrode of type (1) (0.9 cm thick) cycled at 0.6 A (10 mA cm^{-2} at the negative plates): (a) entire cycling, (b) focus on cycles 1 to 6, (c) focus on cycles 18–23. Charges of 2 h with 0.5 L of electrolyte comprising 1 M $Pb(CH_3SO_3)_2$ + 0.25 M CH_3SO_3H + 5 mM HDTMA + 60 mM NaF in the uncharged state.

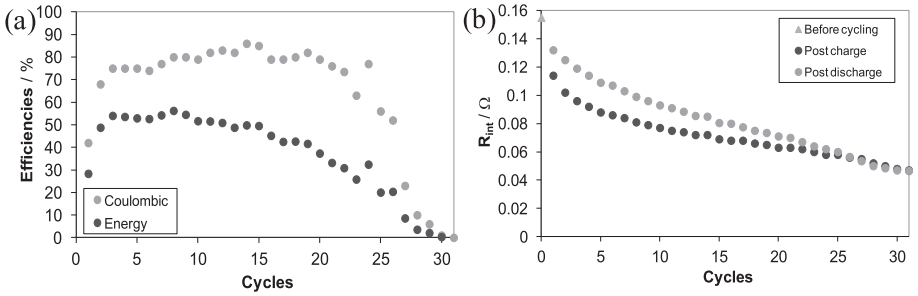

Fig. 7. (a) Coulombic and energy efficiencies and (b) evolution of the internal resistance during the cycling of Fig. 6.

that the F^- ions enhance greatly the adhesion of PbO_2 on the glassy carbon during the deposition/dissolution cycling of the latter [15]. To assess the effect of the incorporation of NaF additive in the electrolyte, a cell comprising a C/C composite positive electrode with L_c = 1.4 cm was cycled using an electrolyte free of NaF. The cycling protocol was the same as in (ii) i.e. 2 h of charge at 0.6 A using 0.5 L of electrolyte.

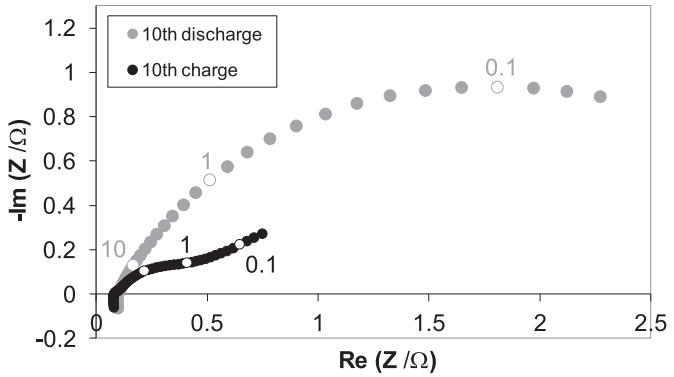

Fig. 8. Impedance spectra recorded at open circuit after the 10th charge and discharge of the cycling described in Fig. 6.

The voltage response of the cell is given in Fig. 9a together with the voltage response of a cell cycled in the same conditions with 60 mM of NaF dissolved in the same electrolyte. As it can be seen, the first charge occurs at a higher voltage (>2 V) in the presence of NaF. However, the voltage progressively decreases to reach the value of 1.9 V at the end of the 1st charge, close to the 1st-charge voltage of the cell cycled without NaF which remains constant. Afterwards, the voltage transients of the two cells are rather similar. Later on during cycling, the drift of the voltage is observed in both cases with a decrease in the efficiencies, as observed previously.

The main benefit of the use of fluoride ions seems to be the enhancement of the PbO_2 cohesion on the positive electrode. As it can be seen in Fig. 9b, the electrolyte without NaF contains many black PbO_2 particles after cycling whereas that containing 60 mM of NaF appears completely translucent and free of detached materials. This confirms that fluoride ions make the lead dioxide more cohesive and more adherent to the vitreous carbon substrate during cycling.

3.1.4. About the poor cyclability of the C/C composite honeycomb electrodes

If it is very likely that the poor cyclability of the cell is directly related to the passivation of the positive electrode upon discharge, the origin of the latter is, however, not clear. It may involve the

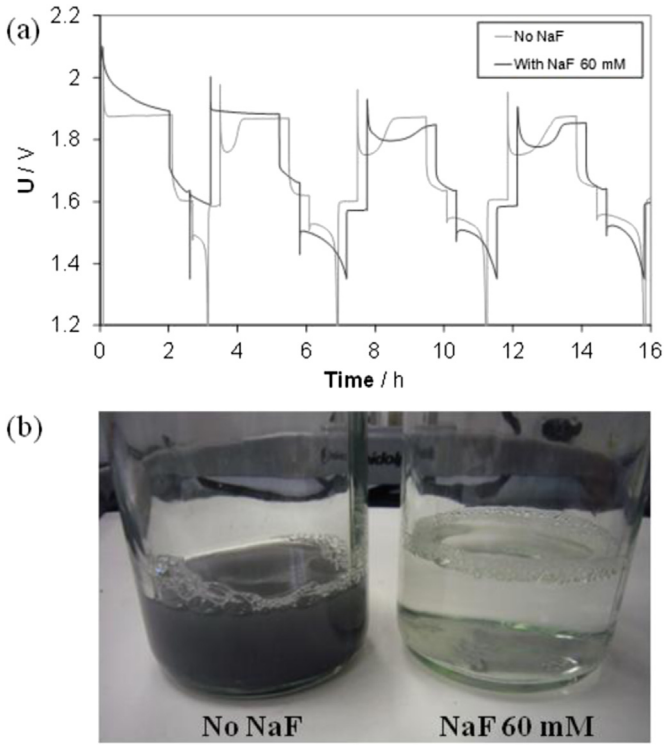

Fig. 9. Effects of the presence in the electrolyte of 60 mM of NaF additives on the cycling properties of the honeycomb cells: (a) voltage responses and (b) electrolyte aspect after cycling.

formation of resistive oxides of lead, referred to as PbO_x [13]. The dissolution of lead dioxide is clearly much more incomplete in the present cell than in any other SLFB flow cell studied in the literature.

The two main differences between the planar SLFB cells reported in the literature and the cell of the present study are, on one hand, the geometry of the positive electrode and, on the other hand, the substrate material used. Considering the geometrical aspect, the three-dimensional honeycomb shape is expected to greatly influence the hydrodynamic of the electrolyte flow, with a heterogeneous flow distribution associated with low convective zones in the alveoli as suggested in our model [14]. Hence, it is possible that a poor flow supply favours the formation of PbO_x and thus inhibits the dissolution of PbO_2. From the material point of view, a relation between the type of substrate and the propensity of PbO_2 to form PbO_x and to subsequently get passivated is not a priori expected, but the C/C composite could degrade upon cycling, especially in contact with the oxidative lead dioxide. If most of the SLFB flow cells studied in the literature comprise a carbon/polymer composite-based positive electrode which is not reported to deteriorate, the observation of the present carbon structure at the end of each experiment strongly suggests that a modification of both its mechanical and electrical properties occurs during cycling. Indeed, by hand, it appeared much more brittle, and electrical path tests carried out with an ohmmeter at many locations of the alveoli structure revealed that the material was much less conductive than before cycling. Unfortunately, any quantitative characterization of the substrate was rendered difficult due to its brittle nature.

To test whether one of these two potential origins of failure (hydrodynamic or substrate material effects) can be validated, a PbO_2 galvanostatic cycling experiment was performed in a 3-electrode electrochemical cell, using a very thin carbon honeycomb sample (2 mm in thickness) as working electrode for the deposition of PbO_2. The cell was filled with ~50 mL of electrolyte solution (composition: 1 M $Pb(CH_3SO_3)_2$ + 0.25 M CH_3SO_3H) which was magnetically stirred under a high rotation rate in order to provide a good convection within the alveoli. The average current density applied to the working electrode was ~2 mA cm^{-2} and the charging time (1 h) implies a very low consumption of soluble lead(II). It appeared that the potential response of the electrode is very similar to that of the cell of Fig. 6. The dissolution potential shifts progressively towards negative values and the cycling cannot be continued any longer after about 20 cycles. The hypothesis of a potential effect of the flow rate is to be excluded due to the fact that the cyclability of PbO_2 is poor even when a high convection is provided to the alveoli. This observation lends strong support to the assumption that the particular carbon-based electrode substrate used in this study is the only responsible for the poor cyclability of the honeycomb cell.

Another PbO_2 cycling experiment in the same 3-electrode cell was conducted using, as the working electrode, a fragment of the electrode frame (~2 mm in thickness, see Fig. 2a) surrounding the alveoli, all other parameters being unchanged. As opposed to the alveoli, a good cycling reversibility was found on this material, with stable charge efficiencies of ~90% for several tens of cycles. A first explanation can be that the thinness of the walls separating the alveoli makes any substantial degradation to happen earlier. But we must also consider that the vitreous carbon constituting the frame and that constituting the alveoli do not come from the same parent material before the carbonisation process: the electrode frame is made of phenolic resin while the honeycomb are made of an aramid material. It is highly possible that the two resulting vitreous carbon materials do not have the same structure, that obtaining by the carbonisation of the phenolic resin being more stable in the oxidative conditions encountered at the positive electrode of a lead flow cell. Identifying (electro)chemical mechanisms responsible for

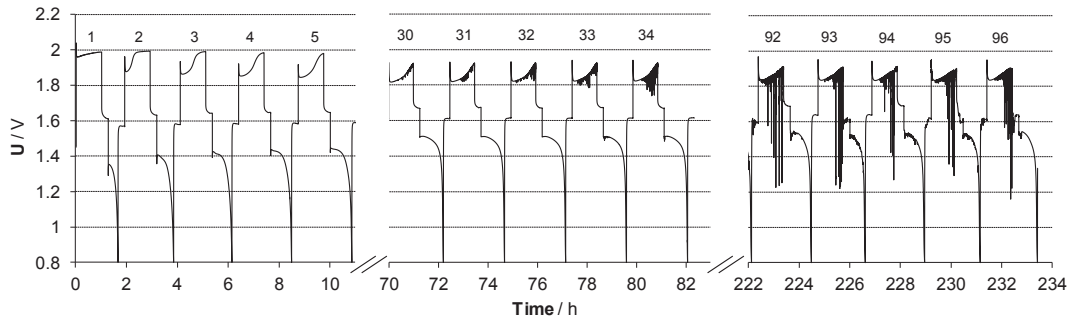

Fig. 10. Voltage response of the cell comprising the graphite positive electrode of type (2) (1.27 cm thick) cycled at 1.2 A (20 mA cm^{-2} at the negative plates). Charges of 1 h with 0.5 L of electrolyte comprising 1 M $Pb(CH_3SO_3)_2$ + 0.25 M CH_3SO_3H + 5 mM HDTMA + 60 mM NaF in the uncharged state.

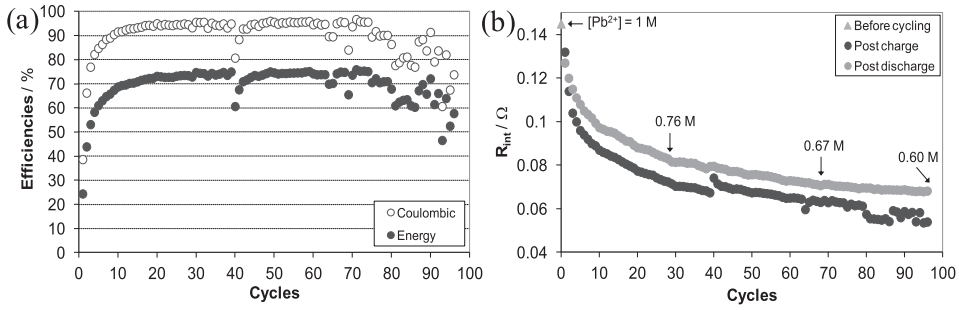

Fig. 11. (a) Coulombic and energy efficiencies and (b) evolution of the internal resistance during the cycling of Fig. 10.

this difference in stability is, however, not the purpose of this paper. Moreover, any surface analysis, after cycling, of the easy-breakable material constituting the alveoli would be particularly difficult without risking to affect its properties, especially because the lead oxide residues are non-adherent to the surface and can shed easily from the surface while extracting fragments for analysis. Anyway, a vitreous carbon such as that synthesised by the protocol described here is not suitable for SLFB application.

3.2. Cells with the graphite "pseudo-honeycomb" positive electrode

To confirm that the C/C composite substrate plays a crucial role in the passivation of the previous SLFB reactors, the positive electrode was replaced by the graphite electrode of type (2). The area ratio R_A of the new cell was estimated to 3, which is three times lower than the ratio that would be developed by the electrode of type (1) comprising the same thickness (1.27 cm).

The cell was cycled at 1.2 A, corresponding to an average current density of 20 mA cm^{-2} at the negative plates and ~7 mA cm^{-2} at the positive electrode. The charges lasted 1 h with the use of 0.5 L of fluorinated electrolyte, involving the deposition of 10% of the active species. The voltage response of the cell is presented in Fig. 10. It can be seen, on one hand, that much more cycles are possible with the graphite electrode. On the other hand, no voltage drifting is observed during the hundred of cycles that were achieved. Rather, the voltage response appears to be very stable and reproducible. In addition, EIS analysis revealed that no passivation occurs after the cell discharge, all of the complex spectra being very close to that recorded after charge and presented in Fig. 8.

The cycling efficiencies are presented in Fig. 11a. The charge efficiency is close to 95% and the energy efficiency to 75% for the majority of the charge/discharge cycles, which is much higher than the efficiencies recorded with the cell comprising the C/C composite honeycomb electrode. It is also 10% points higher than the planar-electrode cell cycled at 20 mA cm^{-2} at the University of Southampton [9]. Clearly, the graphite substrate for the positive electrode brings about a significant enhancement of the global performances of the SLFB cell, as observed by Verde et al. [12] in the case of planar electrodes.

It is also interesting to report on the evolution of the internal resistance of the cell. As it can be seen in Fig. 11b, R_{int} drops substantially during the first cycles but the decaying rate slows down progressively to eventually reach an asymptotical state with a value close to 0.065 Ω. This evolution is again entirely correlated to the evolution of the electrolyte composition which was assessed by titration at regular intervals. The values of the concentration in Pb^{2+}, given in Fig. 11b, show that it has lost 24% of its initial value (1 M) at the 28th cycle (0.76 M), 33% at the 67th cycle (0.67 M) and only 40% by the end of cycling ($[Pb^{2+}] = 0.60$ M at the 96th cycle). The fact that the impoverishment in the soluble lead(II) species slows down throughout the experiment must be related to the increase in the coulombic efficiency, which reaches 95% by the 20th cycle, indicating that much of the deposited material in charge are redissolved in the electrolyte during the following discharge. At this stage, the battery operation can be considered to be quasi-reversible.

However, at the end of cycling, a substantial decrease in the efficiencies must be noted and this seems to be related to some short-circuits between the electrodes, due to the appearance of dendrite-like structures at the negative plates. The latter are responsible for the voltage spikes observed during the charge in the voltage transients of Fig. 10, as soon as the 30th cycle. If there is no indication of any adverse effect of these lead dendrites on the cell performance until the 80th cycle, it is clear that the final decrease in both the coulombic and energy efficiencies is to be ascribed to the short-circuits observed in the voltage response. Despite this, the soluble lead(II) content in the electrolyte remains quite stable as it is observed in Fig. 11b.

Conversely to the planar-electrode cells tested in the literature, the operation of the present cell comprising a 3-D graphite structure for the positive electrode appears to be much more limited by the deposition of dendrite-like structures at the lead negative plates rather than the dissolution process of PbO_2 at the positive electrode.

4. Conclusions

In this study, soluble lead/acid flow cells comprising a 3-D honeycomb-shaped positive electrode were tested in galvanostatic cycling. Two types of substrate were used: type (1) is made of a vitreous carbon/carbon composite material obtained by a carbonisation, under inert atmosphere, of an *Aramid*®/phenolic resin honeycomb block and type (2) consists of a "pseudo-honeycomb" structure comprising circular alveoli drilled in a graphite plate. The two negative electrodes consist of planar plates made of copper sandwiching the honeycomb structure.

The cycling of the cells assembled with a positive electrode of type (1) showed poor performance. For these cells, two failure modes were identified, depending on the cycling conditions. When a high amount of active species are deposited during charge (3 h of charge at 1.7 A), short-circuits are observed early in cycling, which diminishes significantly the performance of the reactor. These short-circuits come from the formation of thick aggregates of lead on the negative plates. When the amount of deposits is reduced (2 h of charge at 0.6 A), a drift in both the charge and discharge voltage is observed upon cycling suggesting the appearance of additional overvoltage. This leads to an increasing loss of energy efficiency. At the end of the cycling, the discharge is even impossible due to a too low voltage. In both cases, the coulombic and the energy efficiencies are very limited, close to 80% and 50%, respectively, and the lifetime of the cell does not exceed 30 cycles. The dissolution of

PbO_2 is particularly limited, bringing about a progressive depletion of the soluble lead(II) ions in the electrolyte together with an increase of the acidity, which makes the electrolyte conductivity to increase and the internal resistance of the cell to decrease. The inability of PbO_2 to be redissolved is associated with the passivation of the positive electrode at the end of discharge. Even if the origin of the passivation is not clear, the deterioration of the C/C composite substrate is likely to be strongly involved in the poor cyclability of the cells. Without improving the cyclability, the use of NaF as an additive in the electrolyte can enhance greatly the adhesion of PbO_2 at the surface of the vitreous carbon honeycomb electrode.

Conversely, when the graphite electrode of type (2) is used, the cyclability is considerably enhanced, even though the geometric surface area of this electrode is not optimised. The coulombic and the energy efficiencies are close to 95% and 75%, respectively, which is 10% points higher than what was reported for planar-electrode cells. No more passivation is observed during the discharge and the number of cycles that can be achieved is in the order of a hundred. The extent to which the system can be cycled is limited by the formation of dendrite-like structure at the negative plate short-circuiting the electrodes.

This work shows that the choice of the positive electrode substrate is crucial for the SLFB and that the use of a graphite-based electrode is particularly promising regarding the performance. Further studies will be needed though to find out more on the mechanisms responsible for the passivation and the degradation of the present C/C composite honeycomb electrodes during the discharge. Also, there is a great need for levelling the lead deposits at the negative plates in order to avoid any dendrites that can short-circuit the graphite-based cells. For this purpose, new material and/or geometry can be tested for the negative electrodes and the geometry of the graphite honeycomb can be further optimised.

References

[1] V. Viswanathan, A. Crawford, D. Stephenson, S. Kim, W. Wang, B. Li, G. Coffey, E. Thomsen, G. Graff, P. Balducci, M. Kintner-Meyer, V. Sprenkle, J. Power Sources 247 (2014) 1040.
[2] A. Hazza, D. Pletcher, R. Wills, Phys. Chem. Chem. Phys. 6 (2004) 1773.
[3] D. Pletcher, R. Wills, Phys. Chem. Chem. Phys. 6 (2004) 1779.
[4] D. Pletcher, R. Wills, J. Power Sources 149 (2005) 96.
[5] A. Hazza, D. Pletcher, R. Wills, J. Power Sources 149 (2005) 103.
[6] D. Pletcher, H. Zhou, G. Kear, J. Low, F.C. Walsh, R. Wills, J. Power Sources 180 (2008) 621.
[7] D. Pletcher, H. Zhou, G. Kear, J. Low, F.C. Walsh, R. Wills, J. Power Sources 180 (2008) 630.
[8] X. Li, D. Pletcher, F.C. Walsh, Electrochim. Acta 54 (2009) 4688.
[9] J. Collins, G. Kear, X. Li, J. Low, D. Pletcher, R. Tangirala, D. Stratton-Campbell, F.C. Walsh, C. Zhang, J. Power Sources 195 (2010) 1731.
[10] J. Collins, X. Li, D. Pletcher, R. Tangirala, D. Stratton-Campbell, F.C. Walsh, C. Zhang, J. Power Sources 195 (2010) 2975.
[11] R. Wills, J. Collins, D. Stratton-Campbell, J. Low, D. Pletcher, C. Walsh, J. Appl. Electrochem. 40 (2010) 955.
[12] M.G. Verde, K.J. Carroll, Z. Wang, A. Sathrumb, Y.S. Meng, Energy Environ. Sci. 6 (2013) 1573.
[13] A. Oury, A. Kirchev, Y. Bultel, E. Chainet, Electrochim. Acta 71 (2012) 140.
[14] A. Oury, A. Kirchev, Y. Bultel, J. Power Sources 246 (2014) 703.
[15] A. Oury, A. Kirchev, Y. Bultel, Patent FR12 57084, deposited on 07/20/2012.
[16] A. Oury, A. Kirchev, Y. Bultel, J. Electrochem Soc. 160 (2013) A148.
[17] D. Pavlov, G. Petkova, J. Electrochem. Soc. 149 (2002) A644.